Electrochimica Acta 121 (2014) 93–101

Contents lists available at ScienceDirect

Electrochimica Acta

journal homepage: www.elsevier.com/locate/electacta

Electrochemical behaviour of gold nanoparticles and Co tetraaminophthalocyanine on glassy carbon electrode

Audacity Maringa, Edith Antunes, Tebello Nyokong*

Department of Chemistry, Rhodes University, Grahamstown 6140, South Africa

ARTICLE INFO

Article history:
Received 9 October 2013
Received in revised form
19 December 2013
Accepted 21 December 2013
Available online 4 January 2014

Keywords:
gold nanoparticles, cobalt tetraaminophthalocyanines, nitrite, electrocatalysis

ABSTRACT

We report on the electrodeposition of gold nanoparticles (AuNPs) onto the glassy carbon electrode (GCE) followed by polymerization of cobalt tetraamino phthalocyanine ($CoPc(NH_2)_4$) on top (represented as poly-$CoPc(NH_2)_4$-/AuNPs-GCE). The modified electrode where $CoPc(NH_2)_4$ is polymerized first followed by deposition of AuNPs is represented as AuNPs/poly-$CoPc(NH_2)_4$-GCE. In the absence of AuNPs, the electrode is represented as poly-$CoPc(NH_2)_4$-GCE or for AuNPs alone (AuNPs-GCE). The surface coverage was 1.5×10^{-9} mol cm^{-2} for AuNPs-GCE and 3.0×10^{-9} mol cm^{-2} for the rest of the modified electrodes. AuNPs/$CoPc(NH_2)_4$-GCE exhibited high electrocatalytic activity towards the oxidation of nitrite, with detection potential of 0.76 V. The catalytic rate constant of 3.96×10^7 cm^3 mol^{-1} s^{-1} was obtained for nitrite oxidation.

1. Introduction

An improvement in electrochemical activity has been observed when bulk electrodes were modified with nanoparticles [1–6]. It has been shown in the review by Campbell and Compton that modification of the inexpensive electrode material with nanoparticles can lead to a larger surface area-to-volume ratio [7]. The nanoparticles enable fast electron-transfer kinetics and this causes a decrease in the overpotential needed for an electrochemical reaction [5]. Gold nanoparticles have been selected in this work because they exhibit good chemical and physical properties, which in turn are dependent on their size, shape and morphology [4]. Gold nanoparticles can be synthesized by chemical [8] and electrochemical methods [1–6]. Electrochemical methods involve the electrodeposition of gold nanoparticles onto substrates such as gold or glassy carbon electrodes. Electrodeposition has been chosen in this work because it is fast, easy and convenient.

Metallophthalocyanines (MPcs) are good electrochemical catalysts. This is due to the accessibility of a range of oxidation states on the Pc unit or on the central metal [9]. The physical and chemical properties of MPcs can be enhanced by varying the substituent on the Pc ring. In this paper we use Co tetraamino phthalocyanine ($CoPc(NH_2)_4$, peripherally substituted), which has been used as an electrocatalyst in a number of reactions including the detection of 2-mercaptoethanol, L-cysteine and nitric oxide just to mention a few [10–12]. The $CoPc(NH_2)_4$ will be deposited onto the glassy carbon electrode by electropolymerization to form poly- $CoPc(NH_2)_4$.

Gold nanoparticles (AuNPs) have been stabilized with thiol or amino phthalocyanines [13–16]. The resulting conjugates were used to detect analytes such as bis phenol A, hydrazine or cytochrome c. The nanoparticles in the reported work [13–16] were synthesized by chemical methods, followed by conjugation to phthalocyanines and the deposition of the conjugates onto the electrode. In the current work, the AuNPs are formed from a gold chloride solution by electrodeposition onto a glassy carbon electrode instead of making them separately using the chemical methods. The $CoPc(NH_2)_4$ will be then be electropolymerized (from dimethylformamide (DMF) solutions) onto the AuNPs using well established methods [17,18]. The attachment of amino groups of $CoPc(NH_2)_4$ onto the AuNPs is also expected. In this paper we explore the effect of polymerizing $CoPc(NH_2)_4$ onto AuNPs modified glassy carbon electrode (GCE) or polymerizing $CoPc(NH_2)_4$ on GCE first followed by electrodepositing gold nanoparticles. Nitrite has been selected as an analyte since $CoPc(NH_2)_4$ is known to catalyse its oxidation [10].

2. Experimental

2.1. Chemicals and reagents

All the chemicals used in this study were of analytical grade and used without further purification. Gold salt ($HAuCl_4$), sodium

* Corresponding author. Tel.:+27 46 603 8260; fax: +27 46 622 5109.
E-mail address: t.nyokong@ru.ac.za (T. Nyokong).

0013-4686/$ – see front matter © 2014 Elsevier Ltd. All rights reserved.
http://dx.doi.org/10.1016/j.electacta.2013.12.132

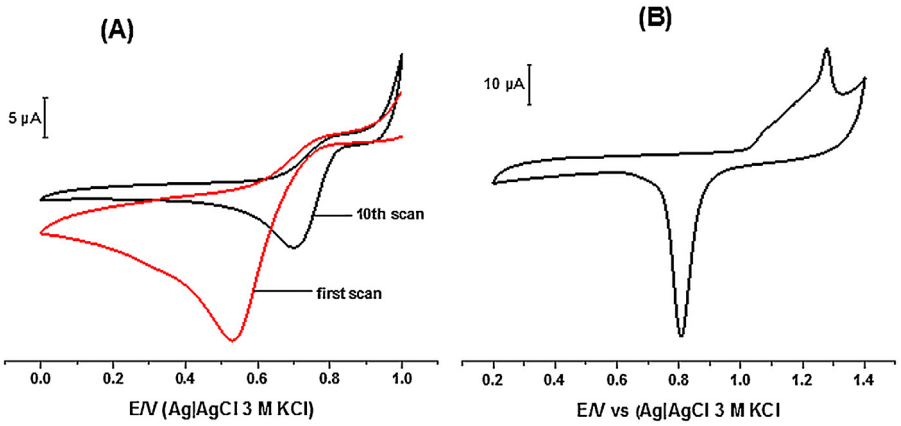

Fig. 1. Cyclic voltammograms (A) of the first and the last scan of 1 mM $HAuCl_4$ in 0.1 M $NaNO_3$. Number of scans: 10, scan rate: 50 mV/s, (B) on AuNPs-GCE recorded in 0.5 M H_2SO_4 solution, scan rate: 100 mV/s.

nitrite, sodium nitrate and pH 4 buffer tablets were purchased from Sigma-Aldrich. Acetone and ethanol were purchased from Saarchem. Tetrabutylammonium tetrafluoroborate ($TBABF_4$) was purchased from Merck. Aqueous solutions were prepared using Millipore water from Milli-Q-Water Systems (Millipore Corp., Bedford, MA, USA). A solution of 1 mM sodium nitrite was prepared in Millipore water. $CoPc(NH_2)_4$ was synthesized as reported in literature [19].

2.2. Equipment

Ultra violet-visible (UV-Vis) absorption spectra were recorded using Shimadzu UV-2550 spectrophotometer. Morphology of the gold nanoparticles were determined by JEOL JEM 1210 transmission electron microscopy (TEM) performed at 100 kV. Scanning electron microscope (SEM) images were obtained using a JOEL JSM 840 scanning electron microscope. Glassy carbon plates (Goodfellow, UK) of 1 × 1 cm and 2 mm thick were used as substrates for SEM. X-ray photoelectron spectroscopy (XPS) analysis was done using an AXIS Ultra DLD, with Al (monochromatic) anode equipped with a charge neutraliser, supplied by Kratos Analytical. The following parameters were used: the emission was 10 mA, the anode (HT) was 15 kV and the operating pressure below 5×10^{-9} torr. A hybrid lens was used and resolution to acquire scans was at 160 eV pass energy in slot mode. The centre used for the scans was at 520 eV with a width of 1205 eV, with steps at 1 eV and dwell time at 100 ms.

Scanning electrochemical microscopy (SECM) experiments were carried out using Uniscan Model 370 equipment and a 15 µm Pt microelectrode (Uniscan) as the tip. SECM approach curves were done using the Pt microelectrode with a Pt counter electrode and Ag|AgCl wire as the pseudo-reference electrode. Images were obtained by maintaining the tip at a constant Z position and scanning in the X–Y plane over the desired area (constant-height mode of SECM) and monitoring changes in the steady-state current of $K_3[Fe(CN)_6]$ oxidation at -0.1 V vs. Ag|AgCl as the tip travels. Glassy carbon plates (Goodfellow, UK) of 1 × 1 cm and 2 mm thick were also used as substrates for SECM.

All electrochemical experiments were performed using Autolab potentiostat PGSTAT 302 (Eco Chemie, Utrecht, The Netherlands) driven by the general purpose Electrochemical System data processing software (GPES, software version 4.9). A three electrode electrochemical cell comprising a glassy carbon electrode (GCE) working, platinum wire counter and Ag|AgCl, 3 M KCl reference electrodes, was employed.

2.3. Electrode preparation and modification

The glassy carbon electrode surface was polished using silicon carbide grinding paper (grit 1200) followed by polishing on a Buehler-felt pad using alumina (0.05 µm). Between each polishing step, sonication for 5 min in absolute ethanol was used to remove any impurity. The electrode was then rinsed with Millipore water and dried under a N_2 stream. This was done to ensure that there are no contaminants on the electrode surface before the electrochemical measurements.

The modification of GCE using gold nanoparticles was done using cyclic voltammetry and a method proposed by Hezard et al. [20]. A deaerated solution of 1 mM $HAuCl_4$ in 0.1 M $NaNO_3$ was cycled at a scan rate of 50 mV/s for 10 scans from 1 V to 0 V. The resulting AuNPs-GCE was then activated using 0.5 M H_2SO_4 by scanning the electrode from 0.2 V to 1.4 V for 10 scans. Separately $CoPc(NH_2)_4$ was electropolymerized on the GCE by continuous cyclic voltammetry of the monomer (1 mM) from −1.2 V to +1.3 V (versus Ag|AgCl) at 100 mV/s for 25 cycles, giving poly-$CoPc(NH_2)_4$-GCE as reported in literature [11,17].

Following the same procedures for preparing the electrode stated above, AuNPs were electrodeposited onto GCE followed by electropolymerization of $CoPc(NH_2)_4$ (represented as poly-$CoPc(NH_2)_4$/AuNPs-GCE). Alternatively, $CoPc(NH_2)_4$ was first electropolymerized followed by electrodeposition of AuNPs (represented as AuNPs/poly-$CoPc(NH_2)_4$-GCE). In summary, the electrodes employed in this work are AuNPs-GCE, poly-$CoPc(NH_2)_4$-GCE, AuNPs/poly-$CoPc(NH_2)_4$-GCE or poly-$CoPc(NH_2)_4$/AuNPs-GCE.

3. Results and Discussions

3.1. Formation and characterization of gold nanoparticles

3.1.1. Electrodeposition and activation

Fig. 1A shows the first and the last cyclic voltammogram of the electroreduction of 1 mM $HAuCl_4$ solution in 0.1 M $NaNO_3$. By cycling the potential from 1 V to 0 V, golden coloured deposits were observed. The forward scan shows the reduction of Au(III) to Au(0) with a cathodic peak at 0.53 V, inducing the deposition of AuNPs onto the GCE surface. This value is very close the one obtained by Hezard and co-workers [20] which was 0.48 V for the reduction of Au(III) on GCE. It can be observed from the cyclic voltammograms that the peak position has shifted to more positive values from 0.53 V to 0.70 V after the 10^{th} scan. This behaviour has been reported before for the formation of AuNPs on GCE [20].

This shift of the reduction peak indicates that on the subsequent scans, the Au deposition occurred on the NPs created during the first scan. Liu and co-workers suggested that the presence of Au nuclei make the deposition of Au easier [21].

The AuNPs-GCE was activated (following literature methods [22]) using 0.5 M H_2SO_4 by cyclising (10 scans) within a potential window from 0.2 V to 1.4 V. Fig. 1B shows the cyclic voltammogram of scan number 10. The anodic and cathodic peaks increased with the increase of the number of scans. The anodic peaks between 1.0 and 1.3 V correspond to Au oxidation. The presence of two peaks is indicative of the formation of different types of Au oxides, mainly AuO according to equation (1) [22].

$$Au + H_2O \rightarrow AuO + 2H^+ + 2e^- \quad (1)$$

The cathodic peak was found at 0.80 V which corresponds to the reduction of oxides formed during the forward scan.

3.1.2. UV-Vis spectra

Fig. 2 shows the absorption spectra of gold nanoparticles in dimethyformamide (DMF). The AuNPs were removed from the GCE by sonicating the AuNPs-GCE in DMF for 5 min. The colour in DMF was pale purple. The surface plasmon absorption resonance peak was obtained at 534 nm. The broad feature between 600 nm and 800 nm is associated with formation of aggregates. Hu and co-workers [6] found out that as the number of cycles increase for the electrodeposition, the peak between 600 nm and 800 nm become more pronounced and they attribute the peak to the formation of aggregates [6], due to the coalescence of adjacent AuNPs with increasing particle size.

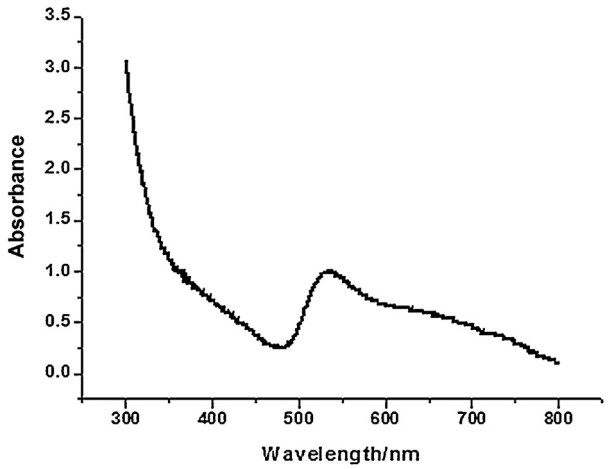

Fig. 2. Absorption spectra of AuNPs in DMF.

3.1.3. TEM images

Fig. 3a shows the transmission electron microscopy (TEM) image of the AuNPs evaporated from DMF solutions. Some

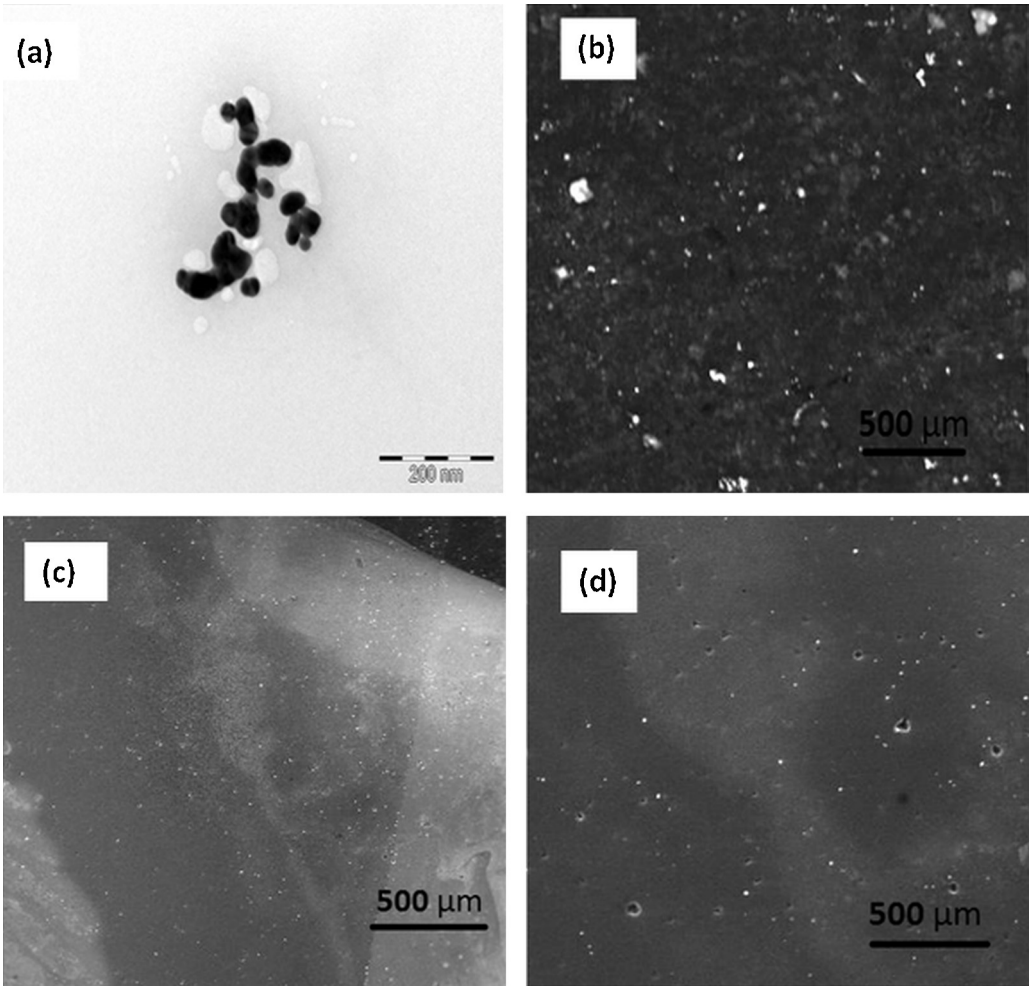

Fig. 3. TEM image of AuNPs evaporated from DMF solutions (a), and SEM image of AuNPs (b), AuNPs/poly-CoPc$(NH_2)_4$ (c) and poly-CoPc$(NH_2)_4$/AuNPs (d) on a glassy carbon plate.

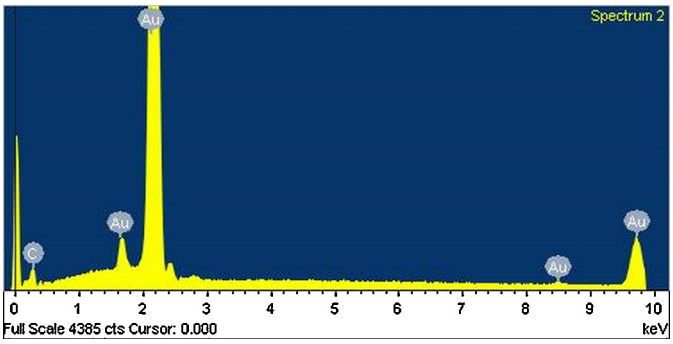

Fig. 4. EDS spectrum of AuNPs on glassy carbon plate.

evidence of agglomeration can be seen on the image. This may be attributed to the number of cycles during electrodeposition as well as the concentration of $HAuCl_4$.

3.2. Characterization of the modified electrodes

3.2.1. SEM images and EDS

Fig. 3 (b-d) shows a scanning electron microscope (SEM) image of AuNPs (b), AuNPs/poly-$CoPc(NH_2)_4$ (c) and poly-$CoPc(NH_2)_4$/AuNPs (d) on a glassy carbon plate. The SEM shows AuNPs of different sizes. As stated above, it has been reported [20] that increasing the number (to over 4) of cyclic voltammetry cycles during the electrodeposition of AuNPs, results in the coalescing of smaller nanoparticles leading to larger nanoparticles, which are less homogenously distributed as observed in Fig. 3b. The SEM image suggests clearly that AuNPs can be deposited on the glassy carbon electrode. When AuNPs are deposited on top of poly-$CoPc(NH_2)_4$, Fig. 3c the nanoparticles were evenly distributed, compared to poly-$CoPc(NH_2)_4$ on top of AuNPs, Fig. 3d, and this will in turn affect electrocatalytic activities.

To further confirm the presence of AuNPs on the glassy carbon plate, energy dispersion spectroscopy (EDS) was used, Fig. 4. The carbon seen on the spectrum is obtained from the glassy carbon plate.

3.2.2. Cyclic voltammetry

$CoPc(NH_2)_4$ was electropolymerized onto the GCE surface using established methods [11,17]. The electropolymerization of $CoPc(NH_2)_4$ onto AuNPs-GCE gave similar voltammograms as reported in literature [11].

Fig. 5 shows the CVs of bare and modified electrodes in 2 mM ferricyanide dissolved in 0.1 M KCl. The anodic and cathodic peak separation (ΔE_p) for bare GCE, AuNPs-GCE, poly-$CoPc(NH_2)_4$-GCE, poly-$CoPc(NH_2)_4$/AuNPs-GCE and AuNPs/poly-$CoPc(NH_2)_4$-GCE are 74 mV, 83 mV, 83 mV, 83 mV and 78 mV respectively at a scan rate of 100 mV/s, Table 1. In terms of electron transfer efficiency the order is bare GCE > AuNPs/poly-$CoPc(NH_2)_4$-GCE > AuNPs-GCE ~ poly-$CoPc(NH_2)_4$-GCE ~ poly-$CoPc(NH_2)_4$/AuNPs-GCE. This confirms good electron transfer kinetics of the bare GCE. AuNPs/poly-$CoPc(NH_2)_4$-GCE has a lower ΔE_p (compared to the rest of the modified electrodes) suggesting fast electron transfer between the redox probe and the electrode modifier.

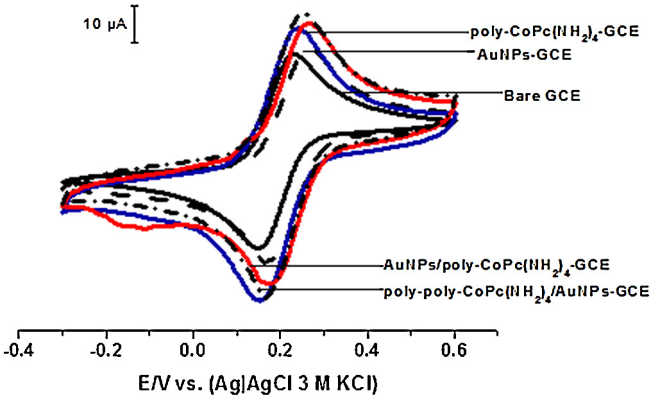

Fig. 5. Cyclic voltammograms of bare and modified GCE in 0.1 M KCl containing 2 mM ferricyanide solution. Scan rate: 100 mV/s.

The surface roughness factor for the modified electrodes were determined using $[Fe(CN)_6]^{3-/4-}$ redox system (Fig. 5) and applying Randles–Sevcik Eq. (2) for reversible systems [23]:

$$I_p = 2.69 \times 10^5 n^{3/2} A_{eff} C D^{1/2} \nu^{1/2} \quad (2)$$

where I_p, n, A_{eff}, C, D and ν are the peak current, the number of electrons involved, the effective surface area, the concentration of $[Fe(CN)_6]^{3-/4-}$, the diffusion coefficient of $[Fe(CN)_6]^{3-/4-}$ and the scan rate, respectively. From the D value for $K_3[Fe(CN)_6] = 7.6 \times 10^{-6}$ cm^2 s^{-1} [24] and n = 1, A_{eff} was estimated to be 0.076 cm^2, 0.092 cm^2, 0.096 cm^2 and 0.10 cm^2 (higher than geometric area = 0.071 cm^2 for a GCE) for AuNPs-GCE, poly-$CoPc(NH_2)_4$-GCE, poly-$CoPc(NH_2)_4$/AuNPs-GCE and AuNPs/poly-$CoPc(NH_2)_4$-GCE respectively, giving roughness factor (= area of modified GCE/area of bare GCE) of 1.07, 1.30, 1.35 and 1.46, respectively. The roughness factors for the poly-$CoPc(NH_2)_4$/AuNPs-GCE and AuNPs/poly-$CoPc(NH_2)_4$-GCE are higher than for the rest of the electrodes due to heterogeneity caused by two different layers (AuNPs and poly-$CoPc(NH_2)_4$).

A linear relationship of peak current versus scan rate (figures not shown) was used to determine the surface coverage of the modified GCE according to the equation (3) [25]

$$I_p = \frac{n^2 F^2}{4RT} \nu A \Gamma \quad (3)$$

where I_p is the background corrected peak current, n is the number of transferred electrons, F is the Faraday constant, Γ is the film surface coverage, A_{eff}, is the effective surface area, v is the scan rate, R is the gas constant and T is the temperature. The values of the surface coverage was found to be 1.5 $\times 10^{-9}$ mol cm^{-2} for AuNPs-GCE, 3.0 $\times 10^{-9}$ mol cm^{-2} for poly-$CoPc(NH_2)_4$-GCE, poly-$CoPc(NH_2)_4$/AuNPs-GCE and AuNPs/poly-$CoPc(NH_2)_4$-GCE. These values are higher than a monolayer surface coverage for a phthalocyanine molecule lying flat [26]. For $CoPc(NH_2)_4$, surface coverage is known to increase with the number of scans [27].

Fig. 6 shows the cyclic voltammograms of bare GCE, AuNPs-GCE, poly-$CoPc(NH_2)_4$-GCE, poly-$CoPc(NH_2)_4$/AuNPs-GCE and AuNPs/poly-$CoPc(NH_2)_4$-GCE recorded in pH 4 buffer at a scan rate of 100 mV/s. pH 4 buffer was chosen since nitrite analysis will be carried out at this pH. AuNPs/poly-$CoPc(NH_2)_4$-GCE showed no peak. Since the poly-$CoPc(NH_2)_4$ layer is under the AuNPs for AuNPs/poly-$CoPc(NH_2)_4$, no peaks due to the $CoPc(NH_2)_4$ were observed, Fig. 6. AuNPs-GCE showed a small anodic peak at 0.89 V this was attributed to the oxidation of AuNPs. The cyclic voltammogram for AuNPs-GCE (in pH 4) differs from one in Fig. 1B due to the conditioning in Fig. 1B and also differences in media. Three processes are observed poly-$CoPc(NH_2)_4$/AuNPs-GCE and two for poly-$CoPc(NH_2)_4$-GCE. The process labelled **II** at $E_{½}$ = 0.37 V and 0.35 V (poly-$CoPc(NH_2)_4$-GCE and poly-$CoPc(NH_2)_4$/AuNPs-GCE respectively) is attributed to Co^{III}/Co^{II} and process **III** at $E_{½}$ = 0.55 V and 0.52 V (poly-$CoPc(NH_2)_4$-GCE and poly-$CoPc(NH_2)_4$/AuNPs-GCE respectively) is attributed to the ring based process [28–30]. Process **I** ($E_{½}$ = 0.16 V) is observed for poly-$CoPc(NH_2)_4$/AuNPs-GCE (and not for poly-$CoPc(NH_2)_4$-GCE). This process may be attributed to the Co^{II}/Co^{I} in comparison with literature [17] but

shifted to more positive potentials in acid media used in this work.

3.2.3. SECM

Fig. 7 shows the 3 D images of unmodified and modified glassy carbon plates (GCP) surfaces. The plates were immersed in an aqueous solution of 2 mM ferricyanide and 0.1 M KCl. The ultramicroelectrode (UME) 15 μm radius Pt, was held at -0.1 V vs Ag|AgCl and brought 10 μm close to the GCP. This resulted in a reduction current corresponding to $[Fe^{III}(CN)_6]^{3-} + e^- \rightarrow [Fe^{II}(CN)_6]^{4-}$. Then, the tip was scanned in the x,y plane (200 μm × 200 μm), ≈ 10 μm above the substrate. From the image in Fig. 7a, it can be seen that the surface of the unmodified plate is smooth and low current was detected. When GCP was modified (Fig. 7b-e), the surface becomes rougher and results in higher currents as compared to the unmodified GCP. AuNPs/poly-CoPc$(NH_2)_4$-GCP (Fig. 7e) had the roughest surface and highest current was detected. The results are well supported by the cyclic voltammetry ferricyanide studies in which AuNPs/poly-CoPc$(NH_2)_4$-GCP had the lowest ΔE_p for the modified GCEs.

3.2.4. XPS

X-ray photoelectron spectroscopy was used to study the surface of unmodified and modified glassy carbon electrodes.

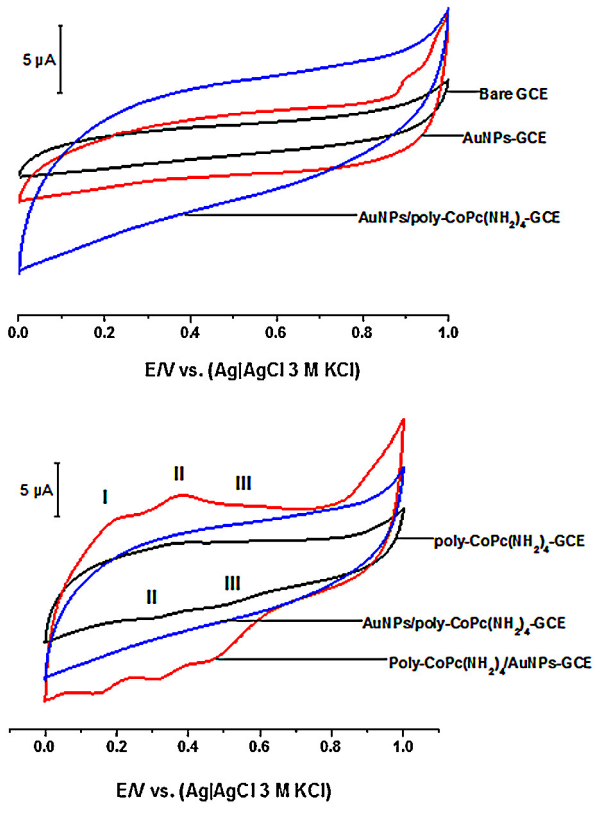

Fig. 6. Cyclic voltammograms of bare and modified GCE recorded in pH 4 buffer. Scan rate: 100 mV/s.

Fig. 8 shows the X-ray photoelectron survey spectra of bare glassy carbon plate (GCP), AuNPs-GCP, poly-CoPc$(NH_2)_4$-GCP, AuNPs/poly-CoPc$(NH_2)_4$-GCP and poly-CoPc$(NH_2)_4$/AuNPs-GCP. The wide scan shows the presence of C (1s) at around 282 eV. The intensity of the peak varies depending on the nature of modification of the GCP. AuNPs/poly-CoPc$(NH_2)_4$-GCP has the lowest C (1s) peak. The gold peaks are observed at 84 eV (4f), 88 eV (4f), 335 eV (4d), 355 eV (4d), 547 eV (4p). They are prominent for AuNPs-GCP and AuNPs/poly-CoPc$(NH_2)_4$-GCP, where the Au is exposed. In poly-CoPc$(NH_2)_4$/AuNPs-GCP, the peaks are weak indicating that the top layer is the one that dominates. Cobalt peaks are observed at 781 eV (2p) and 795 eV (2p). The nitrogen peaks are clearly seen on poly-CoPc$(NH_2)_4$ and poly-CoPc$(NH_2)_4$/AuNPs-GCP at 400 eV (1s). There were no observable peaks of Co on the AuNPs/poly-CoPc$(NH_2)_4$-GCE this is due to the fact that the AuNPs completely cover the surface containing poly-CoPc$(NH_2)_4$. The results are supported by the cyclic voltammogram of AuNPs/poly-CoPc$(NH_2)_4$ in Fig. 6 in which peaks due to CoPc$(NH_2)_4$ were not observed. The samples were all exposed to atmospheric oxygen as a result we observed the presence of oxygen peak at 533 eV (1s).

3.3. Nitrite detection

3.3.1. Cyclic voltammetry

Fig. 9 shows the cyclic voltammograms of bare and modified GCE in 1 mM nitrite in pH 4 buffer. The bare GCE had an oxidation peak at 0.92 V, Table 1. Relative to the bare GCE, the oxidation peak is shifted to lower values for the modified electrodes, Table 1. The peak potential for nitrite oxidation on modified electrodes were 0.83 V, 0.88 V, 0.79 V and 0.76 V for AuNPs-GCE, poly-CoPc$(NH_2)_4$-GCE, poly-CoPc$(NH_2)_4$/AuNPs-GCE and AuNPs/poly-CoPc$(NH_2)_4$-GCE respectively, Table 1. Nitrite oxidation on AuNPs/poly-CoPc$(NH_2)_4$-GCE occurred at a much lower potential of 0.76 V. Higher currents were observed for both AuNPs/poly-CoPc$(NH_2)_4$-GCE and poly-CoPc$(NH_2)_4$/AuNPs-GCE compared to AuNPs-GCE or poly-CoPc$(NH_2)_4$-GCE, showing the advantage of combining the two electrocatalysts (AuNPs and poly-CoPc$(NH_2)_4$). Poly-CoPc$(NH_2)_4$-GCE on its own showed electrocatalysis in terms of peak potential compared to bare GCE, but worse than for the rest of the modified electrodes. Thus the presence of AuNPs enhanced the electrocatalytic oxidation of nitrite. Huang and co-workers found out that the gold nanoparticles play an important role in the oxidation of nitrite by accelerating the rate of electron transfer [5].

3.3.2. Electrochemical impedance spectroscopy (EIS)

The electrochemical behaviour of the different electrodes were further investigated by electrochemical impedance spectroscopy (EIS) in 1 mM nitrite and the results are shown in Fig. 10. Fig. 10a shows the Nyquist plot for the various electrodes that were used in this study. The plots are composed of semi-circles and straight line portions, representing charge transfer (R_{ct}) and diffusion controlled processes, respectively. The Randle equivalent circuit for this process is shown as an inset in Fig. 10a. The equivalent circuit is composed of R_s (the resistance of the electrolyte), in series connection with parallel elements of C_{dl} (double layer capacitance),

Table 1
Electrochemical parameters for the electrode modification and detection of analytes.

Electrode	ΔE/mV (ferricyanide) in 0.1 M KCl	Γ mol cm^{-2} (× 10^{-9})	E_p/V, (nitrite, pH 4)
GCE	74	-	0.92
AuNPs-GCE	83	1.5	0.83
Poly-CoPc$(NH_2)_4$-GCE	83	3.0	0.88
Poly-CoPc$(NH_2)_4$-/AuNPs-GCE	83	3.0	0.79
AuNPs/poly-CoPc$(NH_2)_4$-GCE	78	3.0	0.76

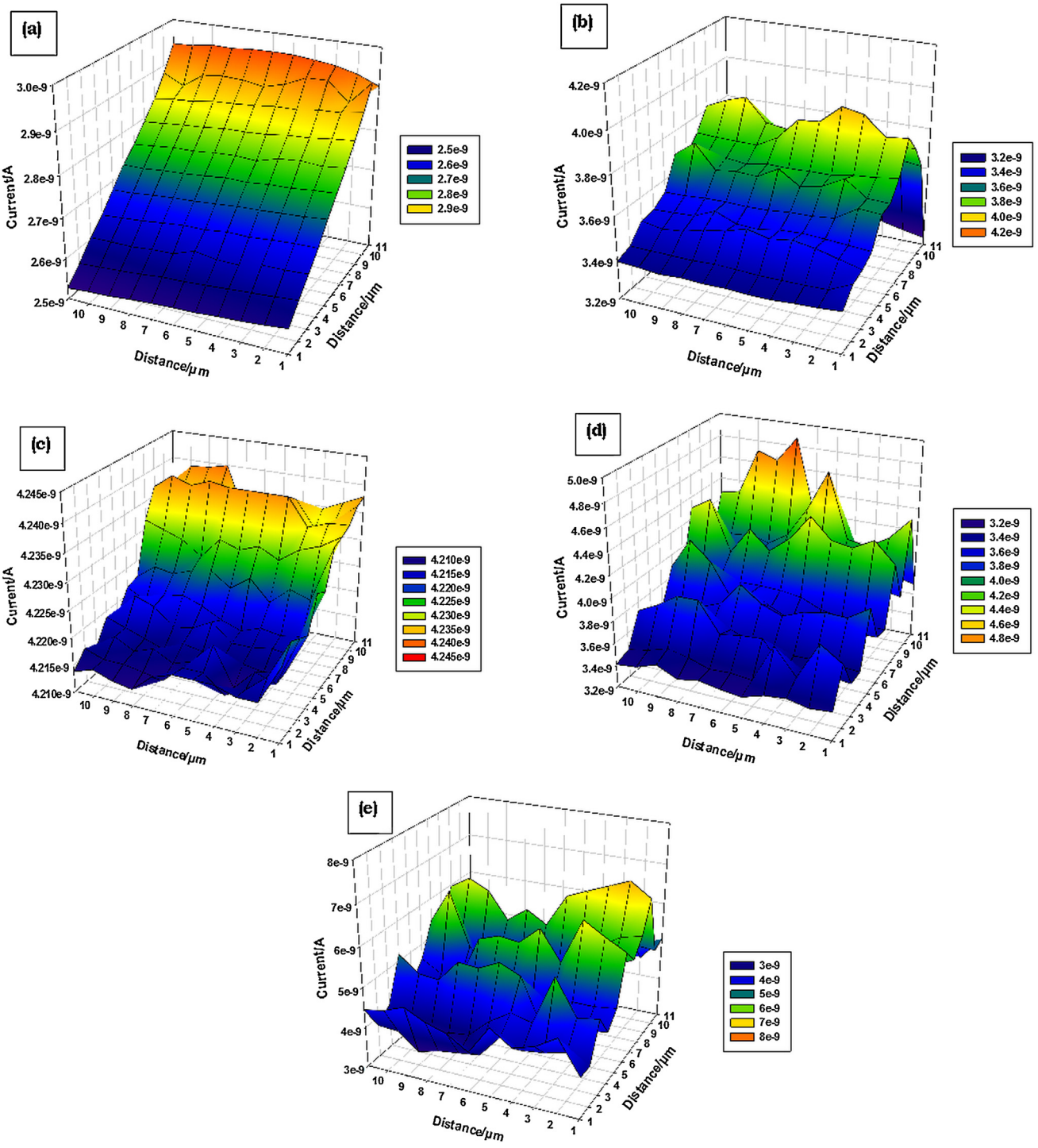

Fig. 7. SECM image of (a) bare GCP, (b) AuNPs-GCP, (c) poly-CoPc$(NH_2)_4$-GCP, (d) poly-CoPc$(NH_2)_4$/AuNPs-GCP (e) AuNPs/poly-CoPc$(NH_2)_4$-GCP in 0.1 M KCl containing 2 mM ferricyanide solution. Imaging conditions: Pt UME (15 μm diameter) placed 10 μm above the substrate, poised at a potential of − 0.1 V vs Ag/AgCl.

R_{ct} (resistance to charge transfer) and Z_W (Warburg impedance). Such circuits have been observed in other studies [31,32]. The R_{ct} as determined by the diameter of the semi-circle was found to be 9.9 kΩ for AuNPs/poly-CoPc$(NH_2)_4$-GCE and is much smaller than that of bare GCE, AuNPs-GCE, poly-CoPc$(NH_2)_4$-GCE and poly-CoPc$(NH_2)_4$/AuNPs-GCE which are 16.6 kΩ, 12.6 kΩ, 13.8 kΩ and 11.1 kΩ respectively, Table 2. This shows that AuNPs/poly-CoPc$(NH_2)_4$-GCE offer limited resistance to charge transfer in the presence of nitrite, hence promoting very fast electron exchange rate, results already confirmed by lower potentials in cyclic voltammetric studies, Fig. 9. The n-values are in the range 0.82–0.87 (n < 1) confirming the non-capacitative nature of the electrodes. Eq. 4 was used to calculate the apparent electron-transfer rate constant (k_{app}) and the results are shown in Table 2.

$$k_{app} = \frac{RT}{F^2 R_{ct} C} \tag{4}$$

where R is the universal gas constant, T is the temperature (298 K), F is the Faraday constant, R_{ct} is the resistance to charge transfer and C is the concentration of nitrite (1 mM). The k_{app} also

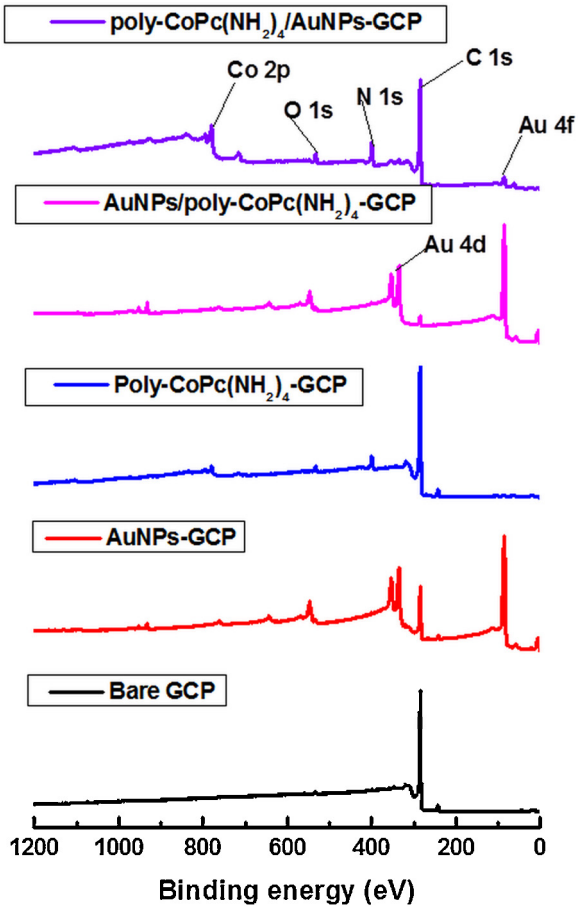

Fig. 8. X-ray photoelectron spectra for bare GCP, AuNPs-GCP, poly-CoPc(NH_2)$_4$ -GCP, AuNPs/poly-CoPc(NH_2)$_4$-GCP and poly-CoPc(NH_2)$_4$/AuNPs-GCP.

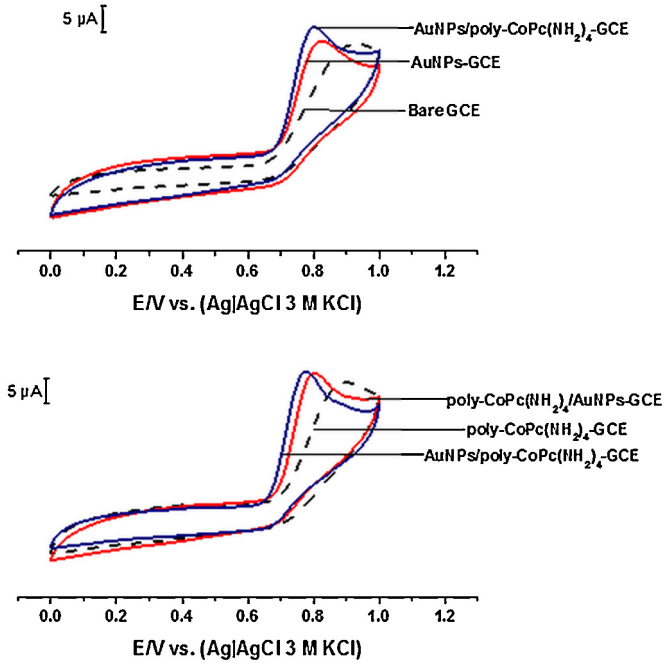

Fig. 9. Cyclic voltammograms of bare and modified GCE recorded in 1 mM nitrite in pH 4 buffer solution. Scan rate: 100 mV/s.

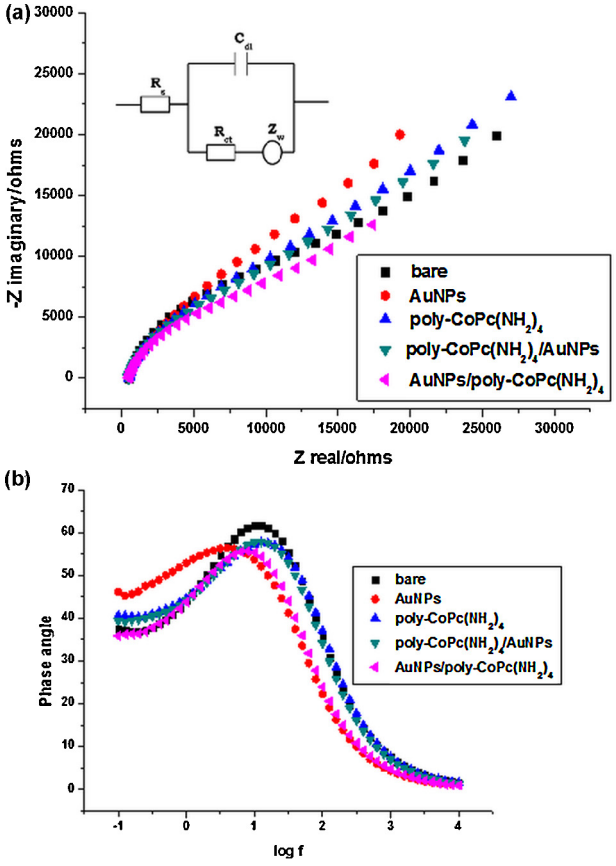

Fig. 10. (a) Nyquist plots obtained for (i) Bare GCE, (ii) AuNPs-GCE, (iii) poly-CoPc(NH_2)$_4$-GCE, (iv) poly-CoPc(NH_2)$_4$/AuNPs-GCE and (v) AuNPs/poly-CoPc(NH_2)$_4$-GCE in 1 mM nitrite (pH 4 buffer). (b) Typical Bode plots obtained for (i) Bare GCE, (ii) AuNPs-GCE, (iii) poly-CoPc(NH_2)$_4$-GCE, (iv) AuNPs/poly-CoPc(NH_2)$_4$-GCE and (v) poly-CoPc(NH_2)$_4$/AuNPs-GCE in 1 mM nitrite (pH 4 buffer).

confirm that the transfer of electrons for nitrite oxidation was faster on the AuNPs/poly-CoPc(NH_2)$_4$-GCE relative to the other electrodes, Table 2. The order in terms of magnitude of k_{app} is as follows: AuNPs/poly-CoPc(NH_2)$_4$-GCE > poly-CoPc(NH_2)$_4$/AuNPs)-GCE > AuNPs-GCE > poly-CoPc(NH_2)$_4$-GCE > bare GCE.

The Bode plot (phase angle (θ) versus log frequency) for the various electrodes is shown in Fig. 10b. Such plots give information which is not easily provided by the Nyquist plot and their nature confirms the structural differences between the modified and the bare GCE. The slight changes in the phase angle and frequencies, compared to bare GCE confirmed that oxidation processes were taking place at the modified surfaces.

3.3.3. Chronoamperometric studies

AuNPs/poly-CoPc(NH_2)$_4$-GCE was employed for these studies due to its superior catalytic activity discussed above. Chronoamperometry data was used to determine catalytic rate constant for the oxidation of nitrite. Catalytic rate constants are a measure of how

Table 2
Impedance data for nitrite detection.

Electrode	R_{ct}/kΩ	n	k_{app}/cm s^{-1}	E vs. (Ag|AgCl)/V
Bare GCE	16.6	0.87	1.61×10^{-5}	0.92
AuNPs-GCE	12.6	0.84	2.11×10^{-5}	0.83
poly-CoPc(NH_2)$_4$-GCE	13.8	0.86	1.93×10^{-5}	0.88
poly-CoPc(NH_2)$_4$/AuNPs-GCE	11.1	0.81	2.40×10^{-5}	0.79
AuNPs/poly-CoPc(NH_2)$_4$-GCE	9.9	0.82	2.69×10^{-5}	0.76

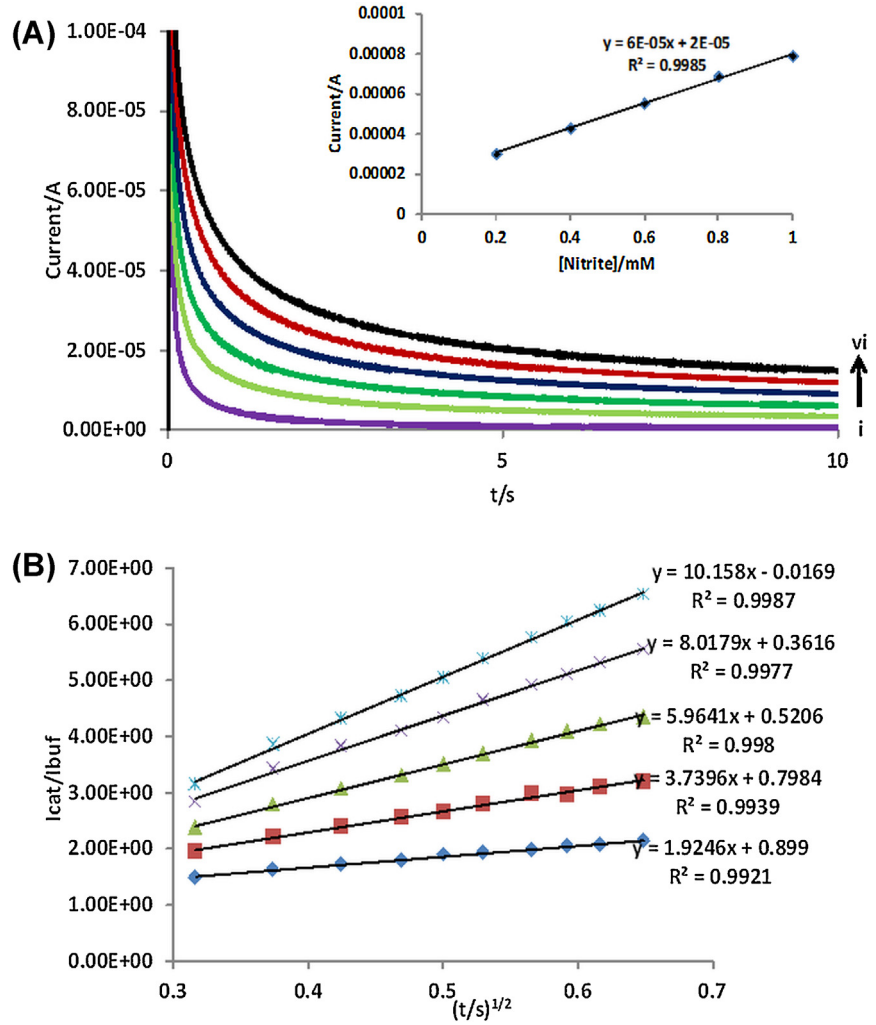

Fig. 11. (a) Chronoamperograms for (i) pH 4 buffer, (ii) 200, (iii) 400, (iv) 600, (v) 800, (vi) 1000 μM nitrite produced on polarized AuNPs/poly-CoPc(NH_2)$_4$-GCE. Inset: current-concentration plot for nitrite. (b) Plot of (I_{cat}/I_{buf}) versus $t^{1/2}$ for (i) 200, (ii) 400, (iii) 600, (iv) 800, (v) 1000 μM nitrite.

fast redox processes takes place at the electrode/analyte interface. Fig. 11A shows the chronoamperometric evolutions on polarized AuNPs/poly-CoPc(NH_2)$_4$-GCE for pH 4 buffer (i) and nitrite (in pH 4 buffer): (ii) 200 μM, (iii) 400 μM, (iv) 600 μM, (v) 800 μM, (vi) 1000 μM. The inset shows a linear relationship between current and concentration and the slope of this plot represent the sensitivity of electrode towards the analyte. Fig. 11B is the plot of (I_{cat}/I_{buf}) versus $t^{1/2}$ (Eq. 5) for nitrite. The catalytic current (I_{cat}) is dominated by the rate at which nitrite is oxidized on the AuNPs/poly-CoPc(NH_2)$_4$-GCE surface. The slopes of the plot of (I_{cat}/I_{buf}) versus $t^{1/2}$ were used to calculate the rate constant according to Eq. (5) [33]

$$\frac{I_{cat}}{I_{buf}} = \gamma^{1/2}\pi^{1/2} = \pi^{1/2}(kCt)^{1/2} \quad (5)$$

where I_{cat} and I_{buf} are currents in the presence and absence of nitrite, respectively, k is the catalytic rate constant, C is the concentration of nitrite and t is the time elapsed in seconds. The plots of the square of slopes obtained from Fig. 11B versus concentration of nitrite were done (figure not shown). A linear relationship was observed and represented by Eq. (6):

$$y = 124.63\,[nitrite]\left(\frac{s^{-1}}{mM}\right) - 30.63\,s^{-1},\ R^2 = 0.9944 \quad (6)$$

where the slope of this plot is equal to πk and the value of k was found to be 3.96×10^7 cm^3 mol^{-1} s^{-1}. The rate constant indicates that AuNPs/poly-CoPc(NH_2)$_4$-GCE was very effective electrocatalysts for the oxidation of nitrite since the value is higher that the reported (= 4.37×10^6 cm^3 mol^{-1} s^{-1}) for nitrite detection on prussian blue nanoparticles modified edge plane pyrolytic graphite [33].

4. Conclusions

AuNPs/poly-CoPc(NH_2)$_4$-GCE and poly-CoPc(NH_2)$_4$/AuNPs-GCE were better electrocatalysts for detection of nitrite than AuNPs-GCE and poly-CoPc(NH_2)$_4$-GCE. In the ferricyanide studies, AuNPs/poly-CoPc(NH_2)$_4$-GCE proved to be the best electrode as it had smallest ΔE_p of 78 mV compared to other modified electrodes. There is enhanced electrocatalytic activity when AuNPs are deposited onto the surface of poly-CoPc(NH_2)$_4$ as seen by the EIS data which showed a small resistance to charge transfer, indicating high transfer rate of electrons. The catalytic rate constant for the detection of nitrite was high 3.96×10^7 cm^3 mol^{-1} s^{-1} as seen in the chronoamperometric studies.

Acknowledgements

This work was supported by the Department of Science and Technology (DST) and National Research Foundation (NRF), South

Africa through DST/NRF South African Research Chairs Initiative for Professor of Medicinal Chemistry and Nanotechnology as well as Rhodes University.

References

[1] Y. Ma, J. Di, X. Yan, M. Zhao, Z. Lu, Y. Tu, Direct electrodeposition of gold nanoparticles on indium tin oxide surface and its application, Biosensors and Bioelectronics 24 (2009) 1480.

[2] L. Wang, W. Mao, D. Ni, J. Di, Y. Wu, Y. Tu, Direct electrodeposition of gold nanoparticles onto indium/tin oxide film coated glass and its application for electrochemical biosensor, Electrochemistry Communications 10 (2008) 673.

[3] J. Wang, L. Wang, J. Di, Y. Tu, Disposable biosensor based on immobilization of glucose oxidase at gold nanoparticles electrodeposited on indium tin oxide electrode, Sensors and Actuators B: Chemical 135 (2008) 283.

[4] M. Etesami, F. Karoonian, N. Mohamed, Electrochemical Deposition of Gold Nanoparticles on Pencil Graphite by Fast Scan Cyclic Voltammetry, Journal of the Chinese Chemical Society 58 (2011) 688.

[5] X. Huang, Y. Li, Y. Chen, L. Wang, Electrochemical determination of nitrite and iodate by use of gold nanoparticles/poly(3-methylthiophene) composites coated glassy carbon electrode, Sensors and Actuators B: Chemical 134 (2008) 780.

[6] Y. Hu, Y. Song, Y. Wang, J. Di, Electrochemical synthesis of gold nanoparticles onto indium tin oxide glass and application in biosensors, Thin Solid Films 519 (2011) 6605.

[7] F. Campbell, R. Compton, The use of nanoparticles in electroanalysis: an updated review, Analytical Bioanalytical Chemistry 396 (2010) 241.

[8] R. Tom, V. Suryanarayanan, P. Reddy, S. Baskaran, T. Pradeep, Ciprofloxacin-Protected Gold Nanoparticles, Langmuir 20 (2004) 1909.

[9] A.B.P. Lever, E.R. Milaeva, G. Speier, in: C.C. Leznoff, A.B.P. Lever (Eds.), Phthalocyanines: Properties and Applications, 3, VCH Publishers, New York, 1993, p. 1.

[10] T. Nyokong, Electrodes modified with monomeric M-N4 catalysts for the detection of environmentally important molecules, in: J.H. Zagal, F. Bedioui, J.-P. Dodelet (Eds.), N4-Macrocyclic Metal Complexes, Springer, USA, 2006, p. 315.

[11] S. Maree, T. Nyokong, Electrocatalytic behavior of substituted cobalt phthalocyanines towards the oxidation of cysteine, Journal of Electroanalytical Chemistry 492 (2000) 120.

[12] J. Jin, T. Miwa, L. Mao, H. Tu, L. Jin, Determination of nitric oxide with ultramicrosensors based on electropolymerized films of metal tetraaminophthalocyanines, Talanta 48 (1999) 1005.

[13] V.P. Chauke, W. Chidawanyika, T. Nyokong, The electrochemical behavior of gold nanoparticle-tantalum (V) phthalocyanine composites: applications towards the electroanalysis of bisphenol A, Electroanalysis 23 (2011) 487.

[14] A.J. Jeevagan, S.A. John, Synthesis of non-peripheral amine substituted nickel(II) phthalocyanine capped gold nanoparticles and their immobilization on electrode for the electrocatalytic oxidation of hydrazine RSC Advances 3 (2013) 2256.

[15] K.S. Lokesh, Y. Shivaraj, B.P. Dayananda, S. Chandra, Synthesis of phthalocyanine stabilized rhodium nanoparticles and their application in biosensing of cytochrome c, Bioelectrochemistry 75 (2009) 104.

[16] K.S. Lokesh, V. Narayanan, S. Sampath, Phthalocyanine macrocycle as stabilizer for gold and silver nanoparticles, Microchimica Acta 167 (2009) 97.

[17] Y. Tse, P. Janda, H. Lam, J.J. Zhang, W.J. Pietro, A.B.P. Lever, Monomeric, Polymeric Tetra-aminophthalocyanatocobalt(II) Modified Electrodes: Electrocatalytic Reduction of Oxygen, Journal of Porphyrins and Phthalocyanines 1 (1997) 3.

[18] P. Mashazi, C. Togo, J. Limson, T. Nyokong, Applications of polymerized metal tetra-amino phthalocya nines towards hydrogen peroxide detection, Journal of Porphyrins and Phthalocyanines 14 (2010) 252.

[19] M. Somashekarappa, J. Keshavayya, S. Sampath, Self-assembled molecular films of tetraamino metal (Co, Cu, Fe) phthalocyanines on gold and silver. Electrochemical and spectroscopic characterization, Pure Applied Chemistry 74 (2002) 1609–1620.

[20] T. Hezard, K. Fajerwerg, D. Evrard, V. Collière, P. Behra, P. Gros, Gold nanoparticles electrodeposited on glassy carbon using cyclic voltammetry: Application to Hg(II) trace analysis, Journal of Electroanalytical Chemistry 664 (2012) 46.

[21] A. Liu, J. Zhu, J. Han, H. Wu, C. Jiang, Fabrication and characterization of gold nanoclusters on phosphorus incorporated tetrahedral amorphous carbon electrode, Electrochemistry communications 10 (2008) 827.

[22] T. Hezard, K. Fajerwerge, D. Evrard, V. Collièree, P. Behra, P. Gros, Influence of the gold nanoparticles electrodeposition method on Hg(II) trace electrochemical detection, Electrochimica Acta 73 (2012) 15.

[23] S. Dong, Z. Jin, Electrochemistry of indium hexacyanoferrate film modified electrodes, Electrochimica Acta 34 (1989) 963.

[24] J. Gooding, V. Praig, E. Hall, Platinum-Catalyzed Enzyme Electrodes Immobilized on Gold Using Self-Assembled Layers, Analytical Chemistry 70 (1998) 2396.

[25] A. Bard, L. Faulkner, Electrochemical Methods, John Wiley and Sons, New York, 2006, pp. 591.

[26] S. Griveau, V. Albin, T. Pauporté, J. Zagal, F. Bedioui, Comparative study of electropolymerized cobalt porphyrin and phthalocyanine based films for the electrochemical activation of thiols, Journal of Material Chemistry 12 (2002) 225.

[27] S. Griveau, J. Pavez, J.H. Zagal, F. Bedioui, Electro-oxidation of 2-mercaptoethanol on adsorbed monomeric and electropolymerized cobalt tetra-aminophthalocyanine films, Effect of film thickness Journal of Electroanalytical Chemistry 497 (2001) 75.

[28] A. Sivanesan, S. John, Amino Group Position Dependent Orientation of Self-Assembled Monomolecular Films of tetraaminophthalocyanatocobalt(II) on Au Langmuir 24 (2008) 2186.

[29] A. Sivanesan, S. John, Adsorption thermodynamics and kinetics study for the self-assembly of 1,8,15,22-tetraaminophthalocyanatocobalt(II) on glassy carbon surface, Electrochimica Acta 54 (2009) 7458.

[30] J. Pillay, K. Ozoemena, Electrochemical properties of surface-confined films of single-walled carbon nanotubes functionalised with cobalt(II)tetraaminophthalocyanine: Electrocatalysis of sulfhydryl degradation products of V-type nerve agents, Electrochimica Acta 52 (2007) 3630.

[31] C. Guo, F. Hu, X. Lou, C. Li, High-performance biofuel cell made with hydrophilic ordered mesoporous carbon as electrode material, Journal of Power Sources 195 (2010) 4090.

[32] M. Pournaghi-Azar, R. Sabzi, Electrochemical characteristics of a cobalt pentacyanonitrosylferrate film on a modified glassy carbon electrode and its catalytic effect on the electrooxidation of hydrazine, Journal of Electroanalytical Chemistry 543 (2003) 115.

[33] A. Adekunle, B. Mamba, B. Agboola, K. Ozoemena, Nitrite electrochemical sensor based on prussian blue/single-walled carbon nanotubes modified pyrolytic graphite electrode, International Journal of Electrochemical Science 6 (2011) 4388.